

Fabrication of hydrogel of hydroxypropyl cellulose (HPC) composited with graphene oxide and its application for methylene blue removal

Xiaoyan Liu^{1,2} · Yifeng Zhou^{1,2} · Wangyan Nie^{1,2} · Linyong Song^{1,2} · Pengpeng Chen^{1,2}

Received: 11 March 2015 / Accepted: 8 June 2015 / Published online: 17 June 2015
© Springer Science+Business Media New York 2015

Abstract Novel environmental friendly hydroxypropyl cellulose (HPC) hydrogels were fabricated upon compositing with graphene oxide (GO) in this work. In order to promote a more homogeneous dispersion of GO sheets in HPC, GO was firstly modified with HPC chains through esterification. The morphology and chemical structure of the functionalized HPC-GO were characterized by transmission electron microscopy, X-ray photoelectron spectroscopy, Fourier transform infrared spectrometer, X-ray diffraction, and thermo-gravimetric analysis. Then scanning electronic microscope was employed to compare the morphologies of the HPC and HPC-GO/HPC hydrogels. The obtained HPC-GO/HPC hydrogels exhibited excellent adsorption performance toward methylene blue. Simulation of the practical use by preparing simple adsorption columns made from in situ formation of HPC-based hydrogels had given a visible observation of the significant adsorption effect brought by the incorporation of HPC-GO sheets. Adsorption kinetics were then imitated by Lagergren pseudo-first-order and pseudo-second-order models. Adsorption isotherms were imitated by Langmuir isotherm and Freundlich isotherm.

Introduction

Recently, tremendous efforts have been devoted to improving the decontamination efficiencies of synthetic dyes, heavy metals, and aromatic pollutants from water because of their detrimental impacts on the environment and human health [1–3]. Technologies actively explored for the removal of these contaminants including biological treatments, liquid membrane separation, coagulation, adsorption, and photocatalytic degradation [4, 5]. Among these methods, adsorption proves to be the most effectively and widely used one because of its relatively low cost, ease of operation, and fewer harmful secondary products. Different adsorbents, such as red mud and fly ash [6], modified silica [7], activated carbon [8], modified alumina [9], polyacrylamide [10], polysaccharide [11], and polybenzimidazole [12], have been utilized for the removal of dyes and heavy metal ions from wastewater. However, these conventional adsorbents are either very costly or hard to be separated or non-degradable. To overcome these problems, it is important to design novel adsorbents with a high adsorption capacity for the removal of contaminants and can be easy retrieved. Most importantly, these adsorbents should be environmentally friendly.

Hydrogels are defined as a three-dimensional cross-linked polymer network structures composed of hydrophilic copolymers. They have been employed as effective adsorbent materials [13–17]. Natural hydrogels made from biopolymers, such as cellulose, chitosan, starch, and alginate, have been considered as potential sorbent materials for dyes and heavy metal removal as they are low cost, biocompatible, and biodegradable than other synthetic hydrogels [18–22]. They are very effective and economical, particularly when used in treating large volume of solutions [23]. A novel adsorbent is prepared via

✉ Yifeng Zhou
yifengzhou@126.com

✉ Pengpeng Chen
chenpp@ahu.edu.cn

¹ School of Chemistry & Chemical Engineering, Anhui University, Hefei 230601, China

² Anhui Province Key Laboratory of Environment-Friendly Polymer Materials, Hefei, China

crosslinking graft copolymerization of 2-(dimethylamino)ethylmethacrylate (DMAEMA) onto carboxymethyl cellulose (CMC) backbone by Ahmed Salama. The CMC-g-PDMAEMA hydrogels are used to remove methyl orange from aqueous solutions, and the high maximum adsorption capacity (1825 mg/g) implies that CMC-g-PDMAEMA can be used as promising adsorbent for the synthetic dyes removal from wastewater [24]. Hydroxypropyl cellulose (HPC) is one of the most important chemical derivatives of cellulose because of its high solubility in water. HPC-based materials are useful in removing dyes from aqueous solutions. However, one of the main limitations in the practical use of HPC hydrogels is their relatively small adsorption capacity [25]. Incorporation of nanofillers with large specific surface and multiple functional groups is often used to improve the adsorption capacity and mechanical properties of the biopolymer-based hydrogels [26, 27].

Graphene oxide (GO), a precursor of chemically converted graphene, has plenty of oxygen atoms on the basal plane and the edge of the sheets in the form of epoxy, hydroxyl, and carboxyl groups [28, 29]. Owing to its large specific area and abundant functional groups, GO has been proven to be a promising material to hybrid with the biopolymer materials for the adsorption use [30]. For instance, a much higher adsorption capacity was obtained when GO was introduced into chitosan hydrogels, and a three-dimensional GO–CS network was formed [31]. Besides, some novel hydrogels based on graphene or graphene oxide have been prepared by Gaoquan Shi and co-workers, and the hydrogels are used as promising adsorbents for the synthetic dyes removal from wastewater [32–34].

Graphene and its derivatives tend to aggregate in a layer-by-layer mode due to strong inter-planar interactions. As a result, when these GO sheets are not dispersed well, a considerable part of their surface area will be lost. To fully exert the effect of graphene oxide, appropriate functionalization of GO for improving its compatibility with polymer matrix is absolutely necessary. Some papers about the noncovalent modification between GO (or RGO) with HPC have been reported [35, 36]. Besides, polysaccharides such as cellulose, chitosan, and cyclodextrin have been covalently grafted onto the surface of graphene nanosheets [37, 38]. HPC has also been covalently grafted to the graphene oxide through the esterification reaction, and the grafting content is close to 30 % [39].

In this paper, a novel microporous GO/HPC hydrogels were fabricated and GO worked as two-dimensional nanofillers with large specific surface and multiple functional groups. In order to promote a more homogeneous dispersion of GO sheets in HPC hydrogels, the GO sheets were firstly grafted with HPC chains. The procedure is

shown in Fig. 1. The functionalization of GO was confirmed via TEM, FT-IR, XPS, and XRD. Morphologies of the as-prepared HPC-GO hydrogels were observed by SEM. Finally, taking methylene blue as a model dye, the adsorption property of the hydrogels was investigated. The adsorption kinetics and isotherms were further studied by fitting the experimental data with different models.

Materials and methods

Materials

Divinyl sulfone (DVS, 97 %) was provided by Sigma-Aldrich. *N*-(3-dimethylaminopropyl)-*N'*-ethylcarbodiimide hydrochloride (EDC·HCl, 98.5 %), 4-dimethylaminopyridine (DMAP, 99 %), and 2-(*N*-morpholino)ethanesulfonic acid (MES, 99 %) were supplied by Aladdin Industrial Corporation. Hydroxypropyl cellulose (HPC, average M_w 100,000) was purchased from Adamas-beta, and graphite power was purchased from Alfa Aesar. Potassium permanganate, sodium nitrate, concentrated sulfuric acid (95–98 wt%), hydrochloric acid (37 wt%), hydrogen peroxide (30 %), and methylene blue (MB) were obtained from Sinopharm Chemical Reagent Co. Ltd. All the chemicals were of analytical grade and used as received.

Preparation of GO

Graphene oxide was prepared by the oxidation of purified natural graphite power according to the modified Hummers method [40]. The details were described as follows [33]. Graphite power (3.0 g) and sodium nitrate (1.5 g) were added to concentrated sulfuric acid (70 mL) under stirring at 0 °C. Then potassium permanganate (9.0 g) was added slowly with stirring during 2–3 h to keep the temperature of the suspension being lower than 20 °C. After increasing the temperature to 35 °C, the reaction system was kept at 24 h. Then, 140 mL of water was added, and the solution was stirred for another 15 min. An additional 500 mL of water was added, followed by a slow addition of 20 mL H₂O₂ (30 %) until the color of the mixture turned to brilliant yellow. The product was filtered and rinsed three times with 1 M HCl solution to remove the metal ions, followed by repeated washing with water and centrifugation to remove the acid. The resulting solid was dispersed in water by ultrasonication for 2 h to make a aqueous dispersion of GO. The obtained brown dispersion was then subjected to 20 min of centrifugation at 4500 rpm to remove any aggregates. Finally, it was purified by dialysis for 1 week to remove the remaining salt impurities for the following experiments.

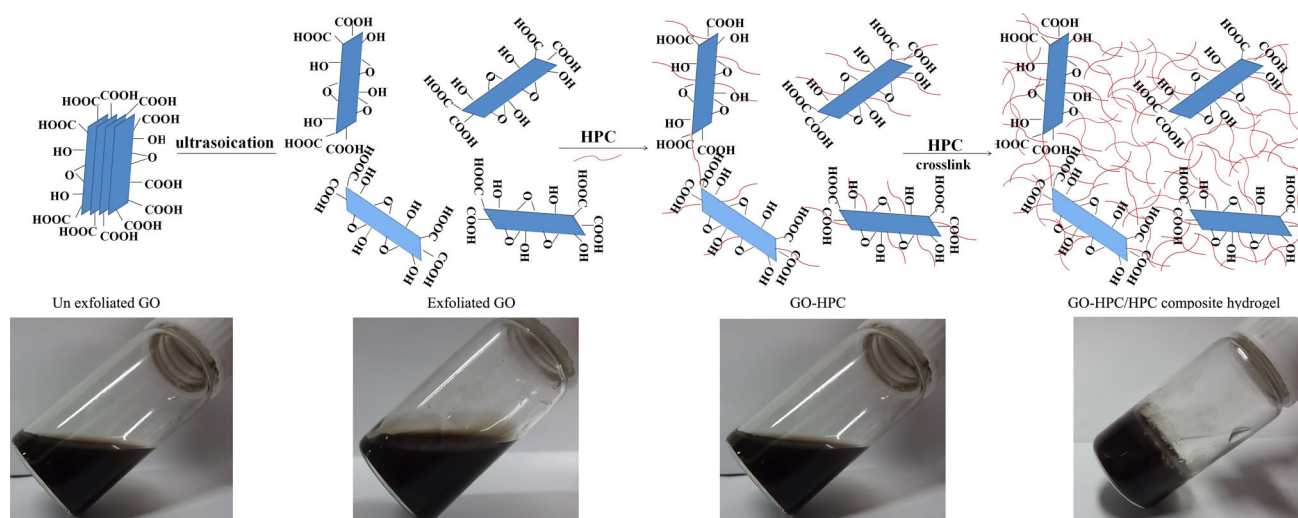


Fig. 1 Scheme for functionalization of GO with HPC and preparation of HPC-GO/HPC hydrogels

Preparation of HPC-GO

HPC-GO was prepared by the esterification of GO with HPC in the presence of EDC·HCl and DMAP. In a typical procedure, 0.1 g GO and 0.1 g HPC were firstly dispersed in 40 mL of deionized water and sonicated for 1 h to get a homogeneous colloidal suspension. 0.12 g EDC·HCl and 0.153 g DMAP were gradually charged into the flask within 20 min. Then 10 mL of MES buffer (0.1 M, pH adjusted to 5) was added to adjust pH to 7. The reaction was conducted at 35 °C under stirring for 48 h. After the reaction was terminated, the suspension was filtered over a 0.45- μm nylon microporous membrane and thoroughly washed with a large amount of deionized water to remove unreacted HPC. Thereafter, the collected solid was redispersed and dialyzed ($MWCO = 14$ kDa) against deionized water for 3 days. The final product was lyophilized.

Preparation of composite hydrogel

To prepare HPC-GO/HPC composite hydrogels, HPC-GO was added to 5 mL of deionized water and sonicated for 1 h to get a homogeneous suspension, and then HPC powder was added to the suspension under stirring to get master batches of 14 wt% HPC-GO/HPC composite solution. Small portions (2 g each) of these batches were removed to individual glass molds, and 50 μL of NaOH (5 M) was added under slowly stirring to ensure uniform mixing while avoiding bubble formation. After white speckles resulted from addition of NaOH disappeared, 12 μL of DVS was added under slowly stirring and the solution was mixed for 2 min. The molds were transferred to a 50 °C water bath and kept for 5 min to firstly crosslink, and then the molds were cooled to 25 °C and continued crosslinking for 24 h

[41], according to the modified temperature-induced phase separation (TIPS) protocol of Gehrke, and co-workers [42] yielded the microporous hydrogels. After termination of crosslinking, the hydrogels were removed into deionized water to dialyze for 48 h.

Characterization

XPS measurements were performed using a Thermo ESCALAB 250 spectrometer. FT-IR spectra of the hydrogels films were recorded on a VERTEX 80+ HYPERION2000 (Bruker, German). XRD patterns were taken on a XD-3 XRD (Beijing Purkinje General Instrument, China) with Cu K α radiation ($\lambda = 1.54$ Å) at an accelerating voltage of 36 kV and a current of 20 mA. Thermo-gravimetric analysis (TGA) was conducted in nitrogen atmosphere with a heating rate of 20 °C/min using a Netzsch TG STA449F3 (Netzsch, German). TEM (JEM-2100, Hitachi) was used to observe the morphology of GO and HPC-GO. The freeze-dried hydrogels were fractured and coated with gold on the surface of the hydrogels. Their surface morphology was observed using a S-4800 FE-SEM instrument (Hitachi, Japan) at a voltage of 3 kV. Water bath sonication was performed with a KQ3200DE sonicator (Kun Shan Ultrasonic Instruments, China) (50 W-33).

Swelling ratio

To investigate the influence of HPC-GO on swelling behavior, the hydrogels were performed in deionized water at 25 °C for 48 h. The hydrogels were taken out and their weight was measured three times until the weight was constant, at which point the swelling equilibrium was reached. The weight ratio, $SR = W/W_0$ (1), was used to

evaluate the swelling ratio, where W was the weight of the swollen hydrogels and W_0 was the weight of the dry hydrogels.

Adsorption experiments

All adsorption experiments were performed on a shaker (Jin cheng Guo sheng, China) with a shaker speed of 120 rpm until the system reached equilibrium. A 100 mL solution of MB and hydrogels were added into 100-mL glass flasks and then shook under 25 °C. At the completion of preset time intervals, MB concentration was measured using a spectrophotometer (UV-1800, Shimadzu, Japan). The maximal absorption peak was 664 nm.

The adsorption amount and adsorption rate were calculated based on the difference of the MB concentration in the aqueous solution before and after adsorption, according to the following equation:

$$Q = \frac{(C_0 - C_e)V}{W_0}, \quad (2)$$

where C_0 and C_e were the initial and equilibrium concentration of MB in milligrams per liter, V was the volume of MB solution, in liters, and W_0 was the weight of the hydrogels used, in grams.

Desorption experiments

The desorption experiments were carried out as follows: the hydrogels were added into 50 mL of 0.5 mol/L HCl for 3 h and then added into water for 10 h after the hydrogels absorbed MB. The hydrogels were reused for adsorption again, and cycles of adsorption–desorption processes were successively conducted three times.

Results and discussion

Characterization of GO–HPC

Figure 2 shows the TEM images of GO and HPC-GO. As shown in Fig. 2a, the graphene oxide was fully exfoliated

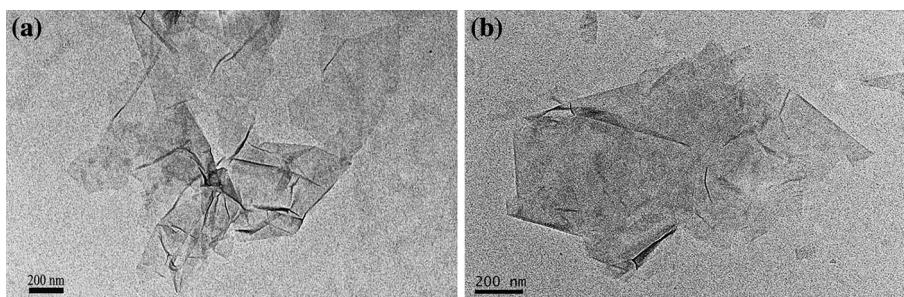
via the modified Hummers method. There were little differences between the morphologies of GO sheets and the HPC-modified ones. It indicated that few aggregation occurred during the functionalization of GO and HPC-GO still kept as monolayer or few layers, which was quite important for the following compositing process.

To further validate the very existence of grafted HPC chains on GO sheets, XPS was used to characterize GO and HPC-GO (Fig. 3). In the XPS spectrum of GO and HPC-GO, two obvious peaks were observed at 284 eV (C 1s) and 531 eV (O 1s). A significant degree of oxidation as numerous oxygen-containing groups was observed in C 1s XPS spectrum of GO (Fig. 3a). From the C 1s XPS spectrum of GO, the C 1s band could be fitted to several components, corresponding to carbon atoms in different positions: C–C/C=C (284.8 eV), C–O (286.8 eV), C=O (287.8 eV), and O–C=O (289 eV) [43]. After modified with HPC, the same oxygen functional groups were still present in C 1s spectrum of HPC-GO (Fig. 3b), but the intensity of the signals attributed to C–O groups increased as a result of the esterification between GO and HPC. It indicated that HPC chains were successfully grafted onto the GO sheets.

The extent of oxidation and esterification of GO were the key parameters to improve their compatibility with the polymer. The oxygen in GO resulted from the oxidation of graphite presented in the form of C–O–C, C=O, and C–OH groups. Figure 4 shows the FT-IR spectra of graphite, GO, HPC, and HPC-GO. FT-IR spectrum of GO (Fig. 4b) revealed several characteristic peaks of oxygen-containing functional groups: peaks at 3420 cm^{-1} and 1383 cm^{-1} corresponded to the hydroxyl (C–OH) group, vibration peak at 1720 cm^{-1} represented the carboxylic group of the oxidized domain, and the peaks at 1225 and 1048 cm^{-1} indicated the presence of C–O–C or C–OH group in GO. Compared to the original GO and HPC, new peak at 1730 cm^{-1} appeared in the FT-IR spectrum of HPC-GO (Fig. 4c), which was the stretching band of the ester groups (–COOR). So the FT-IR results confirmed the successful functionalization of HPC chains onto GO sheets.

Figure 5 depicts the XRD patterns of pristine graphite, GO, HPC, and HPC-GO. The diffraction pattern of pure

Fig. 2 TEM images of GO (a) and HPC-GO (b)



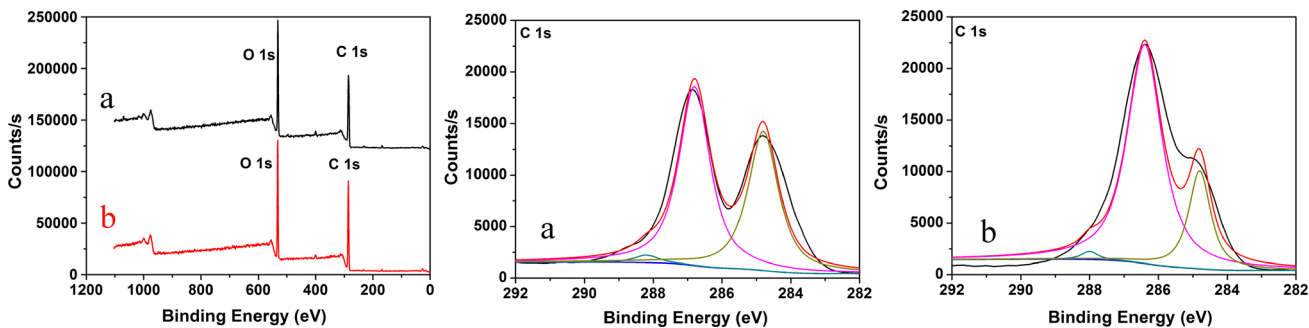


Fig. 3 XPS spectra of GO (a) and HPC-GO (b)

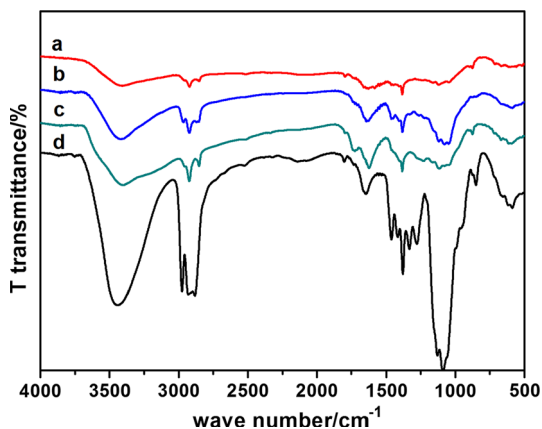
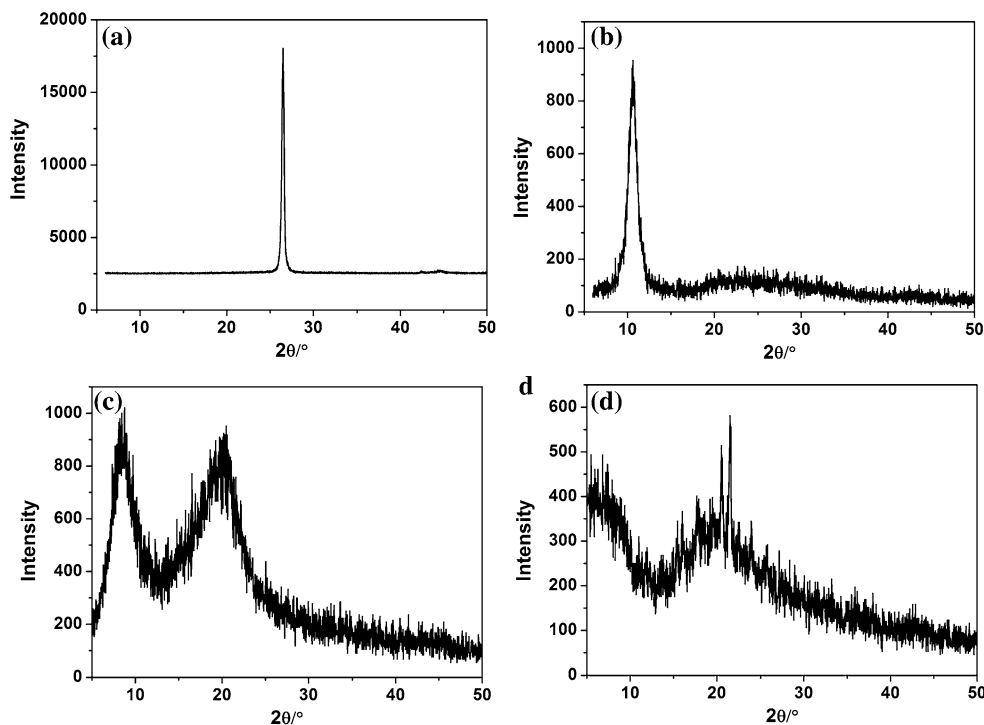


Fig. 4 FT-IR spectra of graphite (a), GO (b), HPC-GO (c), and HPC (d)

GO had a peak at $2\theta = 10.5^\circ$, corresponding to the interplanar distance between GO sheets (Fig. 5b) [1]. The groups caused the GO sheets to stack more loosely, and the interlayer spacing increased from 0.336 nm (26.52°) to 0.833 nm (10.5°). The diffraction angles of HPC-GO (Fig. 5d) were similar to that of the pure HPC (Fig. 5c), and the diffraction peaks corresponding to GO had not been observed. It indicated that the GO sheets were well dispersed in the HPC matrix. Besides, the stronger diffraction intensity of HPC than that of HPC-GO implied a apparently higher crystallinity of the former than the latter, and it revealed that the crystalline degree of HPC decreased after adding to GO [44].

TGA was a complementary technique that could reveal the composition and changes in thermal stability of

Fig. 5 XRD pattern of graphite (a), GO (b), HPC (c), and HPC-GO (d)



samples. The TGA curves of graphite, GO, HPC, and HPC-GO are shown in Fig. 6. TGA traces of pristine graphite showed a negligible weight loss, which was about 0.6 % of its total weight in the entire temperature range (Fig. 6a). Compared with the pristine graphite, GO was thermally unstable and started to lose mass upon heating below 100 °C due to the volatilization of stored water in its π -stacked structure (Fig. 6b) [45]. The major mass loss occurred close to 180 °C, which could be assigned to the pyrolysis of labile oxygen-containing groups. The original HPC started decomposing at 280 °C, and the major mass loss was about at 340 °C (Fig. 6d). After being modified by HPC chains, the weight loss of HPC-GO went to 60 %, whereas that of the unmodified GO was 53 %. The extra weight loss could be attributed to the decomposition of grafted HPC chains on the modified GO sheets.

Characterization of HPC-GO/HPC hydrogels

SEM micrographs of the internal structure of the hydrogels are shown in Fig. 7. A loose 3D network structure with pore sizes of several tens micrometers to hundreds of micrometers was observed from SEM images of HPC hydrogels (Fig. 7a). When composited with HPC-GO, as shown in Fig. 7b, the pore sizes of the HPC-GO/HPC

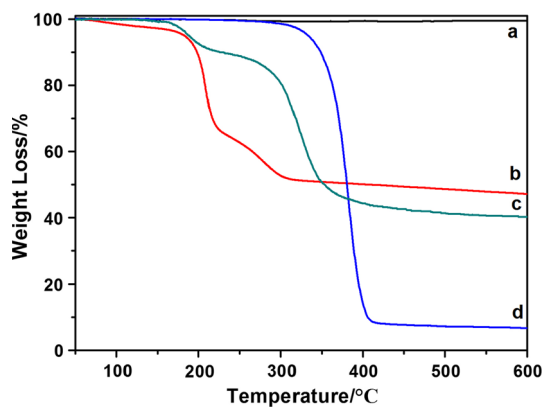
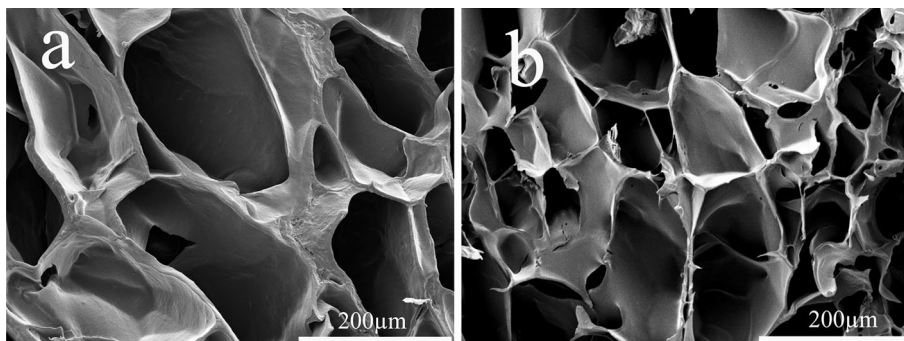


Fig. 6 The TGA of graphite (a), GO (b), HPC-GO (c), and HPC (d)

Fig. 7 SEM images of HPC hydrogels (a) and HPC-GO/HPC hydrogels (b)



hydrogels were obviously smaller. This was because the addition of GO sheets could reduce the expansion of the gel matrixes, resulting in a decrease in the pore sizes [46].

As shown in Fig. 8, the swelling ratios of HPC-GO/HPC hydrogels firstly decreased and then increased. Incorporation of HPC-GO could both increase the crosslink density of HPC hydrogels and introduce many hydrophilic groups. When the added HPC-GO was below 2 wt%, the increased crosslink density played a major role which caused a decrease of swelling ratios of HPC hydrogels. When the added HPC-GO was more than 2 wt%, the introduced hydrophilic groups played a main role which greatly increased the swelling ratios of HPC hydrogels.

Adsorption kinetics

Kinetic study provided important information about the mechanism of MB adsorption, which was necessary to depict the adsorption rate of adsorbent and control the residual time of the whole adsorption process. The pseudo-first-order and pseudo-second-order models were used to fit the experimentally obtained adsorption data. The pseudo-first-order and the pseudo-second-order rate equations were expressed as follows [47].

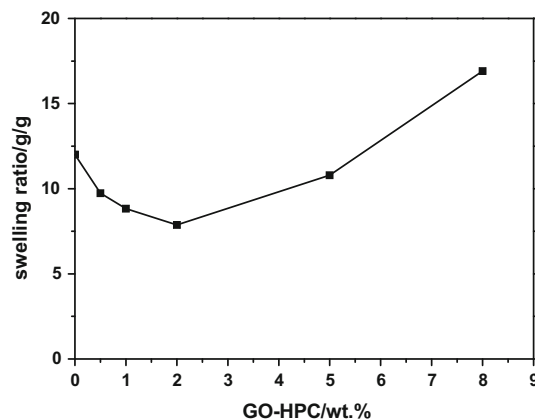


Fig. 8 Swelling ratios of the HPC-GO/HPC hydrogels with different amounts of HPC-GO (wt%) at 25 °C

The pseudo-first-order equation of Lagergren was expressed as

$$\ln(Q_e - Q_t) = \ln Q_e - k_1 t, \tag{3}$$

where Q_e and Q_t were the adsorption amount in mg/g at equilibrium, time ‘ t ’ in min, and k_1 was the rate constant of adsorption (min^{-1}).

The pseudo-second-order equation was expressed as

$$\frac{t}{Q_t} = \frac{1}{k_2 Q_e^2} + \frac{t}{Q_e}, \tag{4}$$

where k_2 was the rate constant for the pseudo-second-order adsorption process.

Figure 9a shows the time profile of MB removal by HPC hydrogels and HPC-GO/HPC hydrogels. As seen, the MB was adsorbed quickly in the first 180 min, and then adsorption became slowly with time, until the adsorption equilibrium was achieved. The adsorption capacity of hydrogels increased with the addition amount of HPC-GO sheets. Photos before and after adsorption by hydrogels with different amounts of HPC-GO were visually compared as shown in Fig. 9b. To simulate the practical use, simple adsorption columns were prepared by in situ formation of HPC and HPC-GO/HPC hydrogels in the centrifuge tubes (Fig. 9c). After the hydrogels were formed, the bottoms of the centrifuge tubes were cut off to allow solution flow down. Then MB solution with a same concentration was poured into the centrifuge tubes. As shown, the solution became clarified after treated by the simple adsorption columns made by HPC-GO/HPC hydrogels, while the solution was still blue after treated by the simple adsorption columns made by HPC hydrogels.

As seen in Fig. 10 and Table 1, the values of experimental Q_e did not agree with the calculated ones, and the values of correlation coefficient (R^2) were relatively low. Compared with pseudo-first-order model (Fig. 10), the higher R^2 value

of pseudo-second-order model (Fig. 11; Table 1) indicated that the pseudo-second-order model was a more applicable model to the kinetics of MB adsorption [48].

The adsorption isotherm

Equilibrium adsorption isotherms reflected the partitioning of dye between the adsorbent and liquid phases at equilibrium as a function of concentration, so they were of prime importance in the design of adsorption systems. The adsorption equilibrium was studied using Langmuir isotherm model and Freundlich isotherm model, respectively [47]. The Langmuir adsorption isotherm was based on the assumption that adsorption took place on homogeneous surface. The equation could be expressed as follows:

$$\frac{C_e}{Q_e} = \frac{1}{k_L Q_m} + \frac{C_e}{Q_m}. \tag{5}$$

The linear form of the Freundlich model could be expressed as follows:

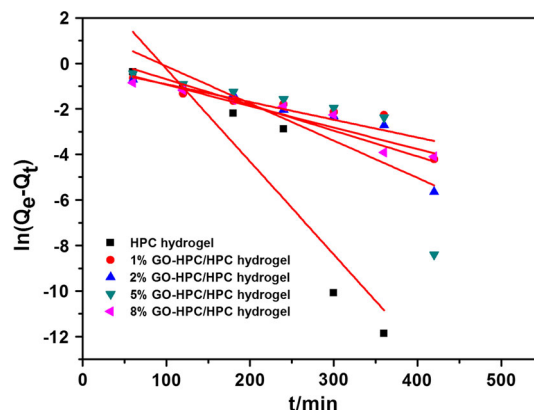


Fig. 10 Pseudo-first-order kinetic plots for the adsorption of MB

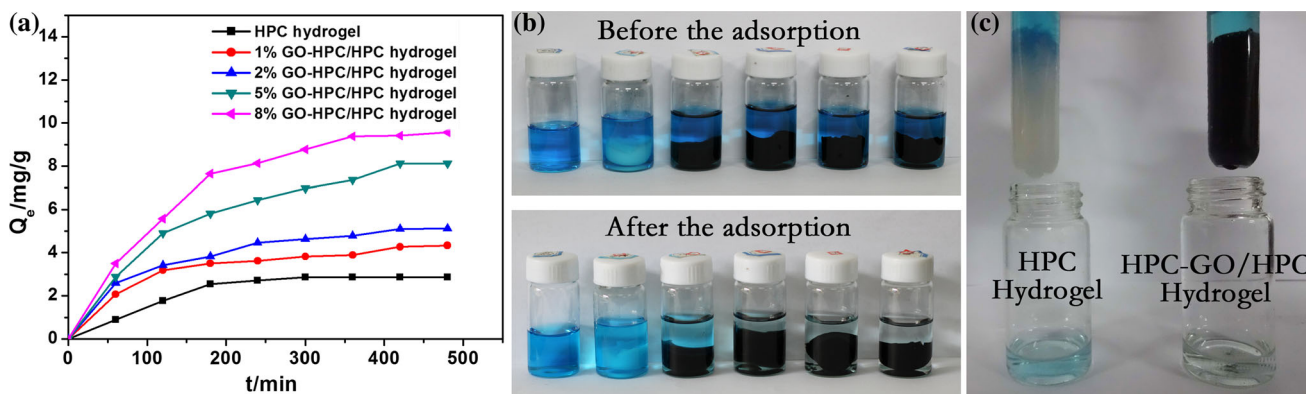
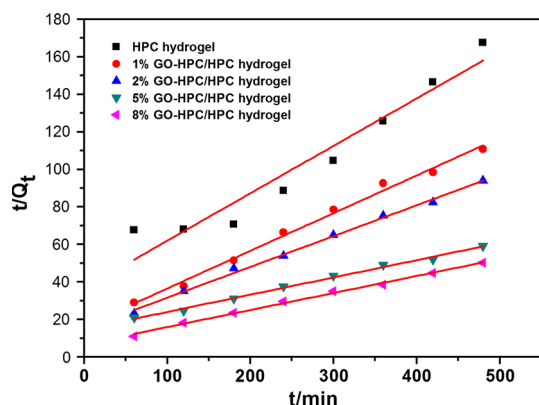


Fig. 9 a Time profile of MB removal on hydrogels. The hydrogels were 0.19 g, and the initial concentration of MB was 50 ppm. b The photos of the hydrogels with different weight ratios of HPC-GO before and after the adsorption. HPC-GO (wt%, from left to right):

blank, 0, 1, 2, 5, 8. c MB removal by simple adsorption columns made by HPC hydrogels and HPC-GO/HPC hydrogels, the time of adsorption was 24 h

Table 1 Adsorption kinetic parameters of MB on hydrogels

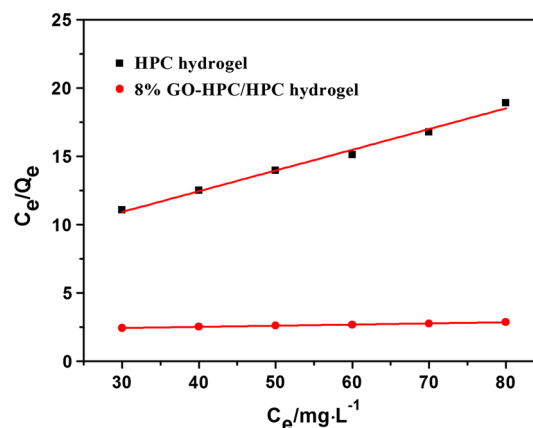
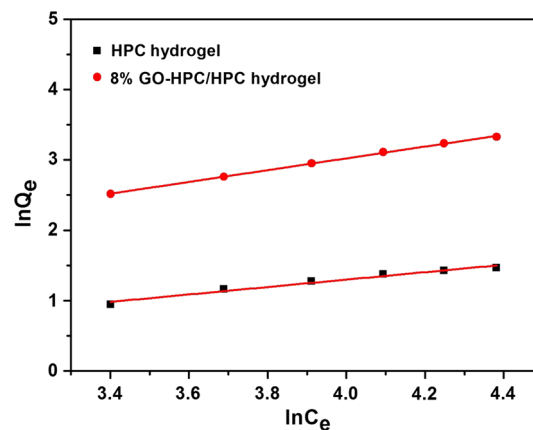
HPC-GO (wt%)	Pseudo-first-order		Pseudo-second-order	
	k_1 (min)	R_1^2	$k_2 \times 10^{-4}$ (g/mg min)	R_2^2
0	0.04075	0.8157	17.38	0.9292
1	0.007790	0.7843	24.57	0.9921
2	0.01132	0.7521	17.81	0.9959
5	0.01635	0.5328	5.740	0.9941
8	0.009440	0.8980	12.06	0.9950

**Fig. 11** Pseudo-second-order kinetics plots for adsorption of MB

$$\ln Q_e = \ln k_F + \frac{1}{n} \ln C_e, \quad (6)$$

where C_e was the equilibrium concentration of MB in aqueous solution (mg/L), Q_e was the adsorption amount (mg/g) at equilibrium, and Q_m was the adsorption capacities of saturation; k_L represented enthalpy of sorption and should vary with temperature, while k_F and n were the Freundlich constants related to the sorption capacity and sorption intensity, respectively.

Both Langmuir and Freundlich equations had been used to analyze the available data, as shown in Figs. 12 and 13. The corresponding parameters for the sample obtained from the lines are listed in Table 2. For HPC hydrogels, R_L^2 was 0.988 and R_F^2 was 0.970. It was shown that the equilibrium adsorption of HPC hydrogels was well described by the Langmuir isotherm model, indicating that the adsorption process was mainly monolayer and took place on homogeneous surface. However, for 8 % HPC-GO/HPC hydrogels, R_L^2 was 0.988 and R_F^2 was 0.999. In addition, the value of experimental adsorption capacity for the adsorption of MB Q_m was 27.849 mg/g, far less than the value calculated from Langmuir model Q_m 118.483 mg/g. It was shown that the equilibrium adsorption of 8 % HPC-GO/HPC hydrogels were well described by the Freundlich isotherm model, indicating that the adsorption process

**Fig. 12** The Langmuir isotherm model for the adsorption of MB on HPC hydrogels and 8 % HPC-GO/HPC hydrogels (The hydrogels were 0.19 g, and the contact time was 24 h.)**Fig. 13** Freundlich isotherm model of MB adsorption for HPC hydrogels and HPC-GO/HPC hydrogels contained 8 wt% HPC-GO (The hydrogels were 0.19 g, and the contact time was 24 h.)

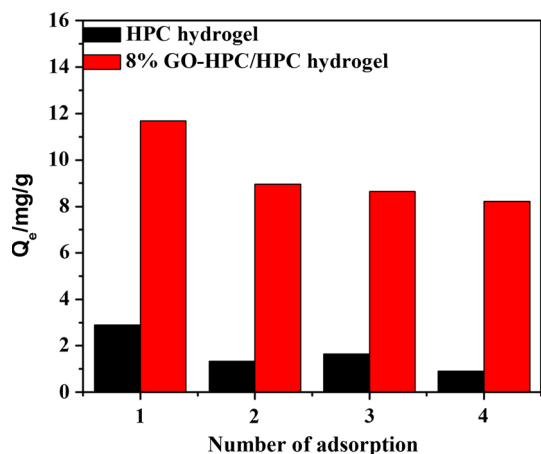
was not monolayer or took place on heterogeneous surface because of the addition of HPC-GO.

Desorption experiments

To evaluate the possibility of regeneration and reusability of hydrogels as adsorbents, desorption experiments were

Table 2 Adsorption isotherm parameters of Langmuir and Freundlich models

HPC-GO (wt%)	Langmuir				Freundlich	
	Q_m (mg/g)	k_L	R_L^2	k_F	n	R_F^2
0	6.596	1.033	0.9886	0.5547	2.115	0.9710
8	118.4	54.28	0.9888	0.7192	1.194	0.9990

**Fig. 14** Adsorption capacity of MB on HPC hydrogel and 8 % HPC-GO/HPC hydrogel in three cycles of desorption–adsorption (The hydrogels were 0.19 g, and the contact time was 10 h.)

performed. Desorption of MB from hydrogels was demonstrated using 0.5 mol/L HCl as an eluent. Cycles of adsorption–desorption experiments were also carried out, as shown in Fig. 14.

The adsorption capacity of HPC-GO/HPC hydrogels was above 70 % of the initial one after desorption for three cycles, while the adsorption capacity of HPC hydrogels was 30 % of the initial one. These results showed that the reusability of GO-HPC/HPC hydrogels was better than that of HPC hydrogels due to the addition of GO-HPC. This could be ascribed to the fact that, in acidic solution, the negatively charged carboxylate anions of GO were protonated and the electrostatic interaction between GO and dye molecules became much weaker [49].

Conclusion

In summary, microporous HPC-GO/HPC hydrogels were prepared and characterized. The hydrogels acted as adsorbents to adsorb MB from aqueous solution, and the results showed that the composite hydrogels had higher adsorption capacity for MB due to the introduction of HPC-GO compared with pure HPC hydrogels. The pseudo-second-order kinetic model well described the adsorption behavior of the MB on hydrogels. The Freundlich isotherm modeled a more applicable model to the equilibrium

adsorption of 8 % HPC-GO/HPC hydrogels, while the Langmuir isotherm model was better for the equilibrium adsorption of HPC hydrogels. Thus, the novel HPC-GO/HPC hydrogels have a great potential to be used as environmentally friendly and economical bio-adsorbent for the removal of dyes from aqueous solution.

Acknowledgements This work was financed by the National Natural Science Foundation of China (Grant No. 51403003), Anhui Provincial Natural Science Foundation (1408085ME86, 1508085QE105), Scientific Research Fund of Anhui Provincial Education Department (KJ2013A014), Startup Foundation for Doctors of Anhui University, Postdoctoral Science Foundation of Anhui Province (01001419), and the 211 Project of Anhui University.

References

- Lei W, Portehault D, Liu D, Qin S, Chen Y (2013) Porous boron nitride nanosheets for effective water cleaning. *Nat Commun* 4:1777. doi:10.1038/ncomms2818
- He F, Wang W, Moon J-W, Howe J, Pierce EM, Liang L (2012) Rapid removal of Hg(II) from aqueous solutions using thiol-functionalized Zn-doped biomagnetite particles. *ACS Appl Mater Interfaces* 4(8):4373–4379. doi:10.1021/am301031g
- Warner CL, Chouyyok W, Mackie KE, Neiner D, Saraf LV, DroubayTC WM, Addleman RS (2012) Manganese doping of magnetic iron oxide nanoparticles: tailoring surface reactivity for a regenerable heavy metal sorbent. *Langmuir* 28(8):3931–3937. doi:10.1021/la2042235
- Wang L (2009) Aqueous organic dye discoloration induced by contact glow discharge electrolysis. *J Hazard Mater* 171(1–3): 577–581. doi:10.1016/j.jhazmat.2009.06.037
- Khin MM, Nair AS, BabuVJ MR, Ramakrishna S (2012) A review on nanomaterials for environmental remediation. *Energy Environ Sci* 5(8):8075–8109. doi:10.1039/C2EE21818F
- Abdel-Halim E (2013) Preparation of starch/poly (N,N-Diethylaminoethyl methacrylate) hydrogel and its use in dye removal from aqueous solutions. *React Funct Polym* 73(11):1531–1536
- Wang WB, TianGY ZZ, Wang AQ (2015) A simple hydrothermal approach to modify palygorskite for high-efficient adsorption of methylene blue and Cu(II) ions. *Chem Eng J* 265:228–238. doi:10.1016/j.cej.2014.11.135
- Malik P (2004) Dye removal from wastewater using activated carbon developed from sawdust: adsorption equilibrium and kinetics. *J Hazard Mater* 113(1):81–88
- Adak A, Bandyopadhyay M, Pal A (2006) Fixed bed column study for the removal of crystal violet (CI Basic Violet 3) dye from aquatic environment by surfactant-modified alumina. *Dyes Pigment* 69(3):245–251
- Paulino AT, GuilhermeMR RA, Campese GM, Muniz EC, Nozaki J (2006) Removal of methylene blue dye from an aqueous media using superabsorbent hydrogel supported on modified polysaccharide. *J Colloid Interface Sci* 301(1):55–62

11. Dehabadi L, Wilson LD (2014) Polysaccharide-based materials and their adsorption properties in aqueous solution. *Carbohydr Polym* 113:471–479. doi:[10.1016/j.carbpol.2014.06.083](https://doi.org/10.1016/j.carbpol.2014.06.083)
12. Khan SB, Lee JW, Marwani HM, Akhtar K, Asiri AM, Seo J, Khan AAP, Han H (2014) Polybenzimidazole hybrid membranes as a selective adsorbent of mercury. *Compos Part B* 56:392–396. doi:[10.1016/j.compositesb.2013.08.056](https://doi.org/10.1016/j.compositesb.2013.08.056)
13. Zheng Y, Zhu Y, Wang A (2014) Highly efficient and selective adsorption of malachite green onto granular composite hydrogel. *Chem Eng J* 257:66–73. doi:[10.1016/j.cej.2014.07.032](https://doi.org/10.1016/j.cej.2014.07.032)
14. Tang QW, Wu JH, Lin JM, Li QH, Fan SJ (2008) Two-step synthesis of polyacrylamide/polyacrylate interpenetrating network hydrogels and its swelling/deswelling properties. *J Mater Sci* 43(17):5884–5890. doi:[10.1007/s10853-008-2857-x](https://doi.org/10.1007/s10853-008-2857-x)
15. Tang QW, Sun XM, Li QH, Lin JM, Wu JH (2009) Synthesis of polyacrylate/polyethylene glycol interpenetrating network hydrogel and its sorption for Fe³⁺ ion. *J Mater Sci* 44(3):726–733. doi:[10.1007/s10853-008-3173-1](https://doi.org/10.1007/s10853-008-3173-1)
16. Wang MQ, Yan J, Du SG, Zeng JW CW, Guo Y, Li HG (2013) Adsorption characteristic of copper ions and its application in electroless nickel plating on a hydrogel-functionalized poly(vinyl chloride) plastic. *J Mater Sci* 48(20):7224–7237. doi:[10.1007/s10853-013-7539-7](https://doi.org/10.1007/s10853-013-7539-7)
17. Ekici S (2011) Intelligent poly(N-isopropylacrylamide)-carboxymethyl cellulose full interpenetrating polymeric networks for protein adsorption studies. *J Mater Sci* 46(9):2843–2850. doi:[10.1007/s10853-010-5158-0](https://doi.org/10.1007/s10853-010-5158-0)
18. Bao Y, Ma J, Li N (2011) Synthesis and swelling behaviors of sodium carboxymethyl cellulose-g-poly(AA-co-AM-co-AMPS)/MMT superabsorbent hydrogel. *Carbohydr Polym* 84(1):76–82. doi:[10.1016/j.carbpol.2010.10.061](https://doi.org/10.1016/j.carbpol.2010.10.061)
19. Pal A, Pan S, Saha S (2013) Synergistically improved adsorption of anionic surfactant and crystal violet on chitosan hydrogel beads. *Chem Eng J* 217:426–434. doi:[10.1016/j.cej.2012.11.120](https://doi.org/10.1016/j.cej.2012.11.120)
20. Zheng Y, Hua S, Wang A (2010) Adsorption behavior of Cu²⁺ from aqueous solutions onto starch-g-poly(acrylic acid)/sodium humate hydrogels. *Desalination* 263(1–3):170–175. doi:[10.1016/j.desal.2010.06.054](https://doi.org/10.1016/j.desal.2010.06.054)
21. Vecino X, Devesa-Rey R, Cruz JM, Moldes AB (2015) Study of the physical properties of calcium alginate hydrogel beads containing vineyard pruning waste for dye removal. *Carbohydr Polym* 115:129–138. doi:[10.1016/j.carbpol.2014.08.088](https://doi.org/10.1016/j.carbpol.2014.08.088)
22. Gao H, Sun Y, Zhou J, Xu R, Duan H (2012) Mussel-inspired synthesis of polydopamine-functionalized graphene hydrogel as reusable adsorbents for water purification. *ACS Appl Mater Interfaces* 5(2):425–432. doi:[10.1021/am302500v](https://doi.org/10.1021/am302500v)
23. Huang X, Liao X, Shi B (2009) Hg(II) removal from aqueous solution by bayberry tannin-immobilized collagen fiber. *J Hazard Mater* 170(2–3):1141–1148. doi:[10.1016/j.jhazmat.2009.05.086](https://doi.org/10.1016/j.jhazmat.2009.05.086)
24. Salama A, Shukry N, El-Sakhawy M (2015) Carboxymethyl cellulose-g-poly(2-(dimethylamino) ethyl methacrylate) hydrogel as adsorbent for dye removal. *Int J Biol Macromol* 73:72–75. doi:[10.1016/j.ijbiomac.2014.11.002](https://doi.org/10.1016/j.ijbiomac.2014.11.002)
25. Yan L, Shuai Q, Gong X, Gu Q, Yu H (2009) Synthesis of microporous cationic hydrogel of hydroxypropyl cellulose (HPC) and its application on anionic dye removal. *Clean* 37(4–5):392–398. doi:[10.1002/clean.200900006](https://doi.org/10.1002/clean.200900006)
26. Faruk O, Bledzki AK, Fink H-P, Sain M (2012) Biocomposites reinforced with natural fibers: 2000–2010. *Prog Polym Sci* 37(11):1552–1596. doi:[10.1016/j.progpolymsci.2012.04.003](https://doi.org/10.1016/j.progpolymsci.2012.04.003)
27. Okamoto M, John B (2013) Synthetic biopolymer nanocomposites for tissue engineering scaffolds. *Prog Polym Sci* 38(10):1487–1503
28. Li D, Muller MB, Gilje S, Kaner RB WG (2008) Processable aqueous dispersions of graphene nanosheets. *Nat Nano* 3(2):101–105
29. Marcano DC, Kosynkin DV, Berlin JM, Sinitskii A, Sun Z, Slesarev A, Alemany LB L, Tour JM (2010) Improved synthesis of graphene oxide. *ACS Nano* 4(8):4806–4814. doi:[10.1021/nn1006368](https://doi.org/10.1021/nn1006368)
30. Zhang Y, Liu J-W, Chen X-W, Wang J-H (2015) A three-dimensional amylopectin-reduced graphene oxide framework for efficient adsorption and removal of hemoglobin. *J Mater Chem B* 3(6):983–989. doi:[10.1039/C4TB01792G](https://doi.org/10.1039/C4TB01792G)
31. Chen YQ, Chen LB, Bai H, Li L (2013) Graphene oxide-chitosan composite hydrogels as broad-spectrum adsorbents for water purification. *J Mater Chem A* 1(6):1992–2001. doi:[10.1039/c2ta00406b](https://doi.org/10.1039/c2ta00406b)
32. Xu Y, Sheng K, Li C, Shi G (2010) Self-assembled graphene hydrogel via a one-step hydrothermal process. *ACS Nano* 4(7):4324–4330
33. Xu YX W, Sun YQ, Bai H, Shi GQ (2010) Three-dimensional self-assembly of graphene oxide and DNA into multifunctional hydrogels. *ACS Nano* 4(12):7358–7362. doi:[10.1021/mn1027104](https://doi.org/10.1021/mn1027104)
34. Bai H, Li C, Wang XL, Shi GQ (2011) On the gelation of graphene oxide. *J Phys Chem C* 115(13):5545–5551. doi:[10.1021/jp1120299](https://doi.org/10.1021/jp1120299)
35. Liao R, Lei Y, Wan J, Tang Z, Guo B, Zhang L (2012) Dispersing graphene in hydroxypropyl cellulose by utilizing its LCST behavior. *Macromol Chem Phys* 213(13):1370–1377. doi:[10.1002/macp.201200137](https://doi.org/10.1002/macp.201200137)
36. Yeo MY, Park SY, In I (2012) Temperature-dependent optical transmittance of chemically reduced graphene oxide/hydroxypropyl cellulose assembly. *Chem Lett* 41(2):197–199
37. Hu HT, Wang XB, Wang JC, Liu FM, Zhang M, Xu CH (2011) Microwave-assisted covalent modification of graphene nanosheets with chitosan and its electrorheological characteristics. *Appl Surf Sci* 257(7):2637–2642. doi:[10.1016/j.apsusc.2010.10.035](https://doi.org/10.1016/j.apsusc.2010.10.035)
38. Xu CH, Wang JC, Wan L, Lin JJ, Wang XB (2011) Microwave-assisted covalent modification of graphene nanosheets with hydroxypropyl-beta-cyclodextrin and its electrochemical detection of phenolic organic pollutants. *J Mater Chem* 21(28):10463–10471. doi:[10.1039/c1jm10478k](https://doi.org/10.1039/c1jm10478k)
39. Yang Q, Pan X, Clarke K, Li K (2011) Covalent functionalization of graphene with polysaccharides. *Ind Eng Chem Res* 51(1):310–317
40. Chen CM, Yang QH, Yang YG, Lv W, Wen YF, Hou PX, Wang MZ, Cheng HM (2009) Self-assembled free-standing graphite oxide membrane (vol 21, pg 3007. *Adv Mater* 21(35):3541–3541. doi:[10.1002/adma.200803726](https://doi.org/10.1002/adma.200803726)
41. Hirsch SG, Spontak RJ (2002) Temperature-dependent property development in hydrogels derived from hydroxypropyl cellulose. *Polymer* 43(1):123–129
42. Kabra BG, Gehrke SH, Spontak RJ (1998) Microporous, responsive hydroxypropyl cellulose gels. 1. Synthesis and microstructure. *Macromolecules* 31(7):2166–2173. doi:[10.1021/ma970418q](https://doi.org/10.1021/ma970418q)
43. Bao HQ, Pan YZ, Ping Y, Sahoo NG, Wu TF, Li L, Li J, Gan LH (2011) Chitosan-functionalized graphene oxide as a nanocarrier for drug and gene delivery. *Small* 7(11):1569–1578. doi:[10.1002/sml.201100191](https://doi.org/10.1002/sml.201100191)
44. Han DL, Yan LF, Chen WF, Li W (2011) Preparation of chitosan/graphene oxide composite film with enhanced mechanical strength in the wet state. *Carbohydr Polym* 83(2):653–658. doi:[10.1016/j.carbpol.2010.08.038](https://doi.org/10.1016/j.carbpol.2010.08.038)
45. Jung I, Dikin D, Park S, Cai W, Mielke SL, Ruoff RS (2008) Effect of water vapor on electrical properties of individual reduced graphene oxide sheets. *J Phys Chem C* 112(51):20264–20268. doi:[10.1021/jp807525d](https://doi.org/10.1021/jp807525d)
46. Shen JF YB, Li T, Long Y, Li N, Ye MX (2012) Study on graphene-oxide-based polyacrylamide composite hydrogels. *Compos Part A* 43(9):1476–1481. doi:[10.1016/j.compositesa.2012.04.006](https://doi.org/10.1016/j.compositesa.2012.04.006)

47. Li L, Luo C, Li X, Duan H, Wang X (2014) Preparation of magnetic ionic liquid/chitosan/graphene oxide composite and application for water treatment. *Int J Biol Macromol* 66:172–178. doi:[10.1016/j.ijbiomac.2014.02.031](https://doi.org/10.1016/j.ijbiomac.2014.02.031)
48. Li LL, Fan LL, Sun M, Qiu HM, Li XJ, Duan HM, Luo CN (2013) Adsorbent for chromium removal based on graphene oxide functionalized with magnetic cyclodextrin-chitosan. *Colloids Surf B* 107:76–83. doi:[10.1016/j.colsurfb.2013.01.074](https://doi.org/10.1016/j.colsurfb.2013.01.074)
49. Namvari M, Namazi H (2014) Synthesis of magnetic citric-acid-functionalized graphene oxide and its application in the removal of methylene blue from contaminated water. *Polym Int* 63(10): 1881–1888